Infrared emission imaging as a tool for characterization of hydrogen storage materials

H. Oguchi[3], E.J. Heilweil[2], D. Josell and L.A. Bendersky[1]
Materials Science and Engineering Laboratory,
[2] Physics Laboratory
National Institute of Standards and Technology,
Gaithersburg, MD 20899. USA
[3] Department of Materials Science and Engineering, University of Maryland, College Park, Maryland 20742, USA

Abstract

Combinatorial thin films provide an opportunity for studying a variety of properties over a wide range of compositions and microstructures on a single substrate, allowing substantial acceleration of both the fabrication and study of materials and their properties. This paper details the use of infra-red (IR) emissivity imaging for studying the in-situ hydrogenation of Mg_xNi_{1-x} films with hydrogen gas; the method is shown to be a powerful combinatorial screening tool for metal hydride storage materials. The 100 nm-thick Mg_xNi_{1-x} composition gradient films ($0.4<x<0.9$) capped with a Pd layer of varying thickness were deposited in a combinatorial electron-beam deposition chamber using a shutter-controlled multilayer technique. The microstructure of as-deposited and 250 ˚C-annealed films was characterized by x-ray diffraction (XRD) and transmission electron microscopy (TEM). TEM studies of the "x-ray amorphous" films shows that the microstructure consists of nano-scale grains of a metastable fcc phase as well as Mg_2Ni and $MgNi_2$ phases over a broad range of higher Ni compositions. The metastable phase appears to be a Ni-stabilized fcc form of Mg. Hydrogenation differences between the studied films and bulk alloys are suggested to be associated primarily with crystallographic differences of the metallic and hydride phases. Hydrogen absorption and desorption of the films were monitored with an infrared camera capable of simultaneously imaging the entire composition spread. The observed changes in infrared intensity during hydrogen loading/unloading demonstrate the sensitivity of the method to hydrogen absorption behavior of different compositions and microstructures.

Keywords: hydrogen storage, combinatorial, IR emissivity, films, Mg-Ni,

[1] Corresponding author. Tel.: 01-301-975-6167, Fax: 01-301-975-4553. E-mail: leoben@nist.gov

1. Introduction

Combinatorial/high-throughput methodologies and tools for accelerated materials research and discovery use discrete composition libraries or continuous composition gradients to study composition–structure–property relationships and to discover new functional materials [1-3]. To investigate specific physical properties of the small volumes of materials, new tools for high-throughput sequential or parallel measurements, different from those used for measuring bulk materials, are often needed. It is thus expected that new measurement tools will continue to emerge as important by-products of combinatorial materials research.

With the recent intensive search for new or improved hydrides to satisfy DOE goals in terms of weight capacity, release temperature and charging/discharging rates [4,5], it is somewhat surprising that combinatorial methods have not been more widely applied to the problem of hydrogen storage materials discovery. Preparation of arrays of varying compositions (combinatorial libraries) is a non-trivial task, but even more difficult is the screening of the arrays for their hydrogen sorption/desorption properties. The standard approach for the search of new hydrogen storage materials is to synthesize bulk samples and to use volumetric [6,7] or gravimetric [8] techniques to follow their hydrogenation reaction and to record pressure–concentration isotherms (p–c isotherms). The equilibrium pressure of the metal-to-hydride transition and thermodynamic parameters are determined from the plateau of the p–c isotherm. So far, no direct methods comparable to the volumetric or gravimetric measurements have been developed for measuring truly combinatorial libraries consisting of a large array of very small amounts of material.

Some research has focused on indirect measurements such as changes in a physical property of a material that coincide with its hydrogenation, to study the hydrogenation process. Olk and co-authors suggested the use of spatially resolved infrared (IR) imaging to observe emissivity changes of Mg–Ni–Fe films due to hydrogen sorption [9]; the approach is based on the fact that metals usually have lower emissivities than insulators. Another research group also used IR imaging as a thermometer to capture heating associated with the formation of hydrides in libraries of multiple samples [10]. Yet another approach has measured changes in stress-state due to hydrogenation of combinatorial thin films; in one example, Ludwig and co-authors measured curvature changes of thin films deposited on micromachined Si cantilevers combinations due to hydrogenation [11].

Arguably the most systematic and comprehensive studies of hydrogenation of combinatorial thin films to date are based on an optical method coined "hydrogenography" [12,13]. This method relies on dramatic changes in optical transparency of a film in response to hydrogen absorption; most complex metal–hydrogen systems undergo a metal–insulator transition upon hydrogen exposure, which result in a significant increase in optical transparency [14,15]. With a straightforward optical setup, hydrogenography makes it possible to simultaneously monitor hydrogen ab- and desorption for thousands of samples at the same time and thus under exactly the same experimental conditions. However, the optical method is much more than a monitoring technique, as it can also provide measurement of thermodynamic parameters.

This paper describes the use of *in-situ* IR imaging to study Mg-based combinatorial thin films during hydrogenation and desorption process. The main goal of the paper is to demonstrate that IR emissivity imaging can accurately capture the response of different materials to hydrogenation process, that the IR intensity correlates with the amount of hydrogen present in the material, and that the IR camera has sufficient spatial resolution to capture differences in the response to hydrogenation for a large number of compositions in films with continuously varying compositions. The work also explores the sensitivity of the method to changes in hydrogenation caused by minor structural modifications. The method is a complementary technique to the aforementioned optical method, namely it also observes changes in electronic characteristics of materials induced by the presence of hydrogen atoms; however the IR measurements do not require optical transparency of the hydrogenated material and can thus potentially be used for a larger class of materials.

Mg and Mg-based alloys were studied because they are of great interest for hydrogen storage research due to the high gravimetric density of hydrogen in MgH_2; the improvement of thermodynamics and kinetics through alloying and structural modification has been studied intensively [16,17]. In addition, there are a number of publications where hydrogenation of Mg and Mg-transition metal films has been studied for improved hydrogenation and for their mirror switching properties [18-30]. In particular Mg [19-23], Mg-Ni and Mg_2Ni, Mg-Ti [24-30] films were recently studied in detail. These publications provide a good reference for the measurements conducted herein.

In general, hydrogenation of the films occurs at temperatures and pressures significantly lower than needed for bulk alloys and exhibits improved kinetics, subject to the *caveat* that the films are typically capped with Pd to promote dissociation of H_2. Reported variations in hydrogenation characteristics can be attributed to variations in microstructures or even in differences in phases in the films due to different deposition methods, conditions and substrates. Most of the Mg films have the crystalline hexagonal close packed structure (hcp) of bulk Mg, either epitaxial single crystals when deposited on an appropriate substrate [19, 21] or columnar grains with [001]-texture [19,23]. Hydrogenation of the Mg films was typically conducted at 80-200 ˚C with H_2 pressure 0.1-0.6 MPa, and hydrogenation time varied from 2 to 90 hours. Studies of films with compositions close to the Mg_2Ni hexagonal phase show that in most cases the [001]-textured nanocrystalline (20-30 nm) Mg_2Ni phase was deposited [25, 27], however depositions of films with compositions between Mg and Mg_2Ni often yielded a structure that, based on x-ray diffraction, was amorphous [24,28]. Hydrogenation of Mg-Ni films was possible at temperatures from 100 to 300 ˚C with pressure from 0.1 to 3.3 MPa. Reported hydrogenation time varied from seconds [29] to hours [30].

2. Link between IR emissivity intensity and hydrogenation.

In thermodynamics, Kirchhoff's law of thermal radiation is a general statement

equating emission and absorption in heated objects, proposed by Gustav Kirchhoff in 1859 [31]. Accordingly, normal spectral emissivity $\varepsilon(\lambda)$ is related to normal spectral reflectivity $R(\lambda)$ as:

$$\varepsilon(\lambda) = 1 - R(\lambda) \qquad (1)$$

The relationship between emissivity and electrical conductivity is determined by fundamental factors including the wave-length of the radiation, and geometrical factors concerned with the experimental arrangement and contributions to the IR signal from surrounding sources. Reflectivity and emissivity in the IR are linked to electrical conductivity via the complex dielectric function. Reflectivity (for normal incidence) depends on the property of material through components of its complex refractive index $N=n+i\kappa$:

$$R = \frac{(n - n_0)^2 + \kappa^2}{(n + n_0)^2 + \kappa^2} \qquad (2)$$

where n is the refractive index, κ is the extinction coefficient, and n_0 is the refractive index of the ambient medium. From this the relationship between emissivity and conductivity can be established [32-34].

In the long wavelength regime (mid- to far-IR, $\lambda>5\mu m$), where the condition $\omega\tau << 1$ is valid (ω is the angular frequency of electromagnetic wave and τ is the relaxation time of the conduction electrons), the Hagen-Rubens relation (for normal incidence of radiation) provides a direct relationship between emissivity and electrical resistivity ρ [32, 33]

$$\varepsilon(\omega) \approx 2\sqrt{2\varepsilon_0 \omega \rho} \qquad (3)$$

where ε_0 is the dielectric constant of vacuum.

Eq. (3) is only for the normal component of the reflectivity and emissivity; however, it can be modified using the concept of complex surface impedance Z to evaluate the emissivity over all angles of emission [34].

From these relations it follows that metals generally have considerably lower emissivities than insulators. The sorption of hydrogen in metals and alloys results in new scattering centers and eventually leads to a modified density of states, which is often accompanied by a rise in the Fermi energy E_f [35,36]. The shift in E_f to an energy with a lower density of states leads to a less metallic character and therefore an increase in the electrical resistance or change of conductivity from metallic to semiconducting or insulating. Thus emissivity is expected to increase with the increase of hydrogen in a material. The link between emissivity in the mid-to-far-infrared regime and electrical conductivity was previously exploited to probe magnetoresistance [37]; a direct relationship between the change in radiated flux and giant magnetoresistance was confirmed experimentally.

3. Experimental

Mg_xNi_{1-x} composition spread thin films of 100 nm thickness were deposited on thermally oxidized Si(100) substrates using a multilayer-deposition technique in a combinatorial electron-beam evaporator deposition chamber [38]. Motion of a shadow mask during deposition created a pair of complimentary wedge-like layers of each target. Films for study were fabricated by sequential deposition of hundreds of such layers. The thickness of the wedge-like layer is a key factor in realizing complete mixing of the layers; it was determined via cross-sectional transmission electron microscopy (TEM) that atomic-scale mixing of the Mg-TM (TM – transition metals) systems could be achieved with the layers less than or equal to 0.5 nm-thick at their thickest portion. Typical dimensions of the thin films studied are 13 mm (length) × 8 mm (width) × 100 nm (thickness). The deposited films were protected from oxidation by deposition of an overlayer of Pd (without vacuum break) deposited at room temperature, which also acts as a catalyst for H_2 dissociation. Some composition spreads were capped with a uniform 5 nm-thick Pd layer while others were capped with a wedge-like layer of Pd, its thickness varying from 0 to 20 nm in the direction orthogonal to the direction of the compositional gradient. The specimens with wedge-like Pd layer were used to determine the optimal thickness of Pd needed to activate hydrogenation. To study the effect of microstructural differences on hydrogenation, one Mg_xNi_{1-x} film was annealed in the deposition chamber at 250 ºC for 2 hours immediately after deposition prior to being capped with Pd.

The compositional variation in the films was measured by energy dispersive spectroscopy (EDS). The measurement shows near-linear variation of composition that is consistent with the deposition parameters. A Bruker-AXS D8 DISCOVER scanning x-ray microdiffractometer with area detector was used to characterize the phases present in the film along a compositional spread[2]. For each sample, 10 equally spaced measurement points encompassing the entire composition gradient were studied.

High-resolution TEM was performed to analyze microstructural details at several selected positions (compositions) of the composition spreads in order to clarify the XRD results. Cross-sectional TEM specimens were prepared using the standard procedure of cutting, gluing, slicing, grinding, dimpling, and ion milling, the last using 5 keV Ar ions at angles of 2 to 8˚ in a Precision Ion Polishing System. The cutting and dimpling procedure was performed in hexane. TEM specimens were examined using a JEM 3010UHR TEM operating at 300 kV.

Hydrogen absorption/desorption of the films was studied by acquiring IR images of the film surface during hydrogen exposure. The samples were set in a hydrogenation chamber, clamped to a heating stage, and IR emission images were collected every 30 seconds through a sapphire window. The IR camera employs a 256x256 array of InSb diodes, which are electrically biased to permit “snap-shot” imaging (with 10 microsecond or longer integration times). The camera has peak sensitivity at a wavelength of 5 micrometers, but is able to detect over an integrated range of 1.0 to 5.5 μm. The acquired

[2] Names of equipment and manufacturers are provided for completeness of description only; they do not imply NIST endorsement.

IR emission images were analyzed post acquisition with image analysis software to extract the temporal evolution of each intensity pixel to obtain the evolution of IR intensity for each film composition and thickness.

In order to eliminate factor that might affect IR intensity but are not related to hydrogenation, e.g., temperature fluctuations, normalized IR intensities were used (IR intensity of the thin films divided by IR intensity from a fixed region that is inert to hydrogenation, e.g., stainless steel surface of a heater or open Si substrate). Evolutions of the normalized IR intensity with time (and changing hydrogenation conditions, such as pressure and temperature) were obtained for 30 measurement points (compositions) along the composition gradient of each specimen.

4. Results

4.1 Structural characterization of the films.

Composition variations of the studied films are shown in Fig. 1. The measurement points are 1 mm apart along a composition gradient across the entire spread. All samples show near-linear variation of composition along the target composition range (Mg fraction x) $0.4<x<0.95$, with good run-to-run reproducibility.

Scanning XRD θ-2θ measurements are shown in Fig. 2 a,b for as-deposited and 250 ˚C annealed films, respectively. Each figure consists of 10 scans taken from the 10 measurement points of different compositions. The scans are offset to allow comparison of results for multiple compositions, with the higher scans having the higher Mg composition. The Si(400) peak from the substrate and the Pd(111) peaks from the overlayer are seen at 69.1 º and 40.1 º, respectively, for all the samples. For the as-deposited Mg_xNi_{1-x}, (Fig. 2(a)), no clear peaks from either the equilibrium Mg or intermetallic Mg_2Ni or $MgNi_2$ phases were observed, suggesting that the entire composition range has a metastable "XRD-amorphous" or nano-crystalline structure. XRD scans of the 250 ºC-annealed Mg_xNi_{1-x} film, Fig. 2b, shows the appearance a broad peak at 44 º for higher Ni concentrations (x=0.4 to 0.5). The peak can be assigned to the (114) of $MgNi_2$. The differences in the XRD patterns suggest that some structural modification took place as a result of 250 ºC annealing. The broad peak around 55 to 57 ˚ was found to belong to the substrates.

In order to clarify the nature of the "XRD-amorphous" microstructure, cross-sectional TEM samples from as-deposited and 250 ˚C-annealed films were examined by conventional and high-resolution TEM. TEM results for three compositions, approximately 21, 43 and 60 at % Ni, are shown in Fig. 3. Figure 3a is a bright field image of the 21 at% Ni cross-section, in which uniformity of composition across the film thickness, a 10 nm-thick capping layer of Pd and a featureless amorphous SiO_2 substrate can be seen. Diffraction contrast variations of the film suggest (nano)crystalline rather than amorphous structure, and this is supported by the selected area electron diffraction (SAED) patterns taken from all three cross-sections of the film (Fig. 3b-d).

Analysis of the SAED patterns shows the presence of continuous diffuse diffraction rings in all three patterns. The sequence and measured d-spacing of the rings allow the rings to be indexed to an fcc structure with lattice parameter a = 0.43 nm. For higher Ni compositions additional diffractions spots are seen, especially between the (002) and (220) fcc rings. These reflections are consistent with reflections of either Mg_2Ni or $MgNi_2$ compounds, although no reflections of the larger d-spacings from these phases are observed. Confirmation of the metastable fcc structure also comes from high-resolution phase-contrast imaging. Fig. 4a shows the microstructure of a 43 at% Ni section at the interface with a SiO_2 substrate. It is clear that the SiO_2 is amorphous, whereas the film consists of randomly oriented crystallites of 5-8 nm in size. Fast Fourier Transform (FFT) of the high-resolution image (Fig. 4c) shows two rings of spots corresponding to (111) and (002) reflections of the fcc structure, as it was identified from the SAED patterns. Fig. 4b shows a high-resolution image of a grain oriented with a [011] zone axis parallel to the electron beam. FFT of the image in Fig. 4d confirms the fcc structure.

The microstructure of the as-deposited films was studied less extensively by TEM. Nevertheless, SAED patterns of selected cross-sections indicate that the as-deposited films have similar fcc structure in a broad range of compositions. The fcc phase coexists with equilibrium intermetallic phases Mg_2Ni and $MgNi_2$ at compositions with Ni>40 at%.

4.2 Infrared characterization of hydrogenation and desorption process of the films.

Fig. 5a,b compares two IR images acquired before and after hydrogenation: image (a) was taken after the sample was equilibrated at 150 ˚C for one hour in vacuum, and image (b) was taken after the sample was exposed at 150 ˚C to hydrogen at 0.5 MPa (5 bar) pressure for 3 hours. The orientation of the compositional gradient (90 to 40 at% Mg) and variations in thickness of the Pd layer (0 to 20 nm) are shown in Fig. 5a. Two effects not related to hydrogenation are observed: decrease in intensity for higher Ni concentration, and lower intensity for thicker Pd. There is no obvious difference between the two images; the effect of hydrogen on the IR intensity is only apparent when the evolution in normalized intensity is viewed over numerous frames during the 10-hour long hydrogenation/desorption experiments.

Evolution of normalized IR intensities with time during the experiments is shown for the as-deposited and 250 ˚C annealed films in Fig. 6a and b, respectively. In these experiments the films were equilibrated in vacuum at 150 °C prior to exposing the samples to hydrogen, thus the change in the films' IR emissivities during hydrogenation could be attributed primarily to the reaction of the films with hydrogen gas. Thirty equally spaced points along the composition gradient, with Pd thickness of approximately 10 nm, were selected in the acquired IR images. The schedule of the experiment is shown at the top of each figure and includes stabilization at 150 ˚C in a 10^{-4} Pa vacuum, step-wise increasing pressure of hydrogen from vacuum to 0.5 MPa, step-wise decrease of pressure back down to vacuum, and then heating to 200 ˚C. Figure 6 shows the evolution

of IR intensity with time for the selected compositions; the curves are offset for viewing, with higher Mg composition at the top.

There is a clear increase of IR intensity immediately after the start of hydrogenation as well as a decrease to the near-pre-hydrogenation level during desorption in vacuum. For the as-deposited film, Fig. 6a, the increase and decrease of IR intensity is most pronounced for the high Mg compositions $x > 0.8$. For these compositions the increase almost completed at 0.1 MPa pressure. For the lower Mg compositions ($x < 0.7$) there is a secondary increase in intensity when hydrogen pressure reaches 0.5 MPa. Decrease of IR intensity occurs only after removing the hydrogen in vacuum. The compositions that exhibit the secondary increase of intensity show an intensity drop (hydrogen desorption) at 150 ºC (between 6 to 7 h) whereas the higher Mg compositions exhibit the decrease in intensity only after increase of temperature to 200 ºC (7 to 10 h). At 200 °C the slope of the intensity decrease with time is higher for higher Mg concentrations, probably because hydrogen in this material was not released at the preceding 150 °C.

To study the effect of different microstructures on hydrogen absorption/desorption, the same set of experimental conditions was applied to the 250 ºC-annealed Mg_xNi_{1-x}. Figure 6(b) shows the normalized IR intensity data for the film. In general, the trend in intensity changes is similar to that of as-deposited Mg_xNi_{1-x}: intensity changes more rapidly for higher concentrations of Mg and the major intensity increase occurs at hydrogen pressure 0.1 MPa (1 to 2 h). Different behavior was measured for the 250 ˚C-annealed films was as follow: The major IR intensity increase occurs at 0.1 MPa (1 to 2 h), with gradual increase at higher pressures. No secondary increase in intensity for lower Mg compositions was observed. IR intensity started to decrease when hydrogen pressure was dropped to 0.1 MPa at 150 °C, with additional decrease at vacuum. No additional decrease in intensity was measured when the temperature was increased to 200 °C.

The significant difference between the two Mg_xNi_{1-x} samples is that the IR intensity for the higher Mg concentrations decreased with decrease of hydrogen pressure at 150 °C for the annealed film as compared to 200 °C for the as-deposited film, i.e., a lower desorption temperature for the annealed film. The differences may come from the differences in microstructures of as-deposited and annealed Mg_xNi_{1-x}, suggesting the importance of microstructural control.

5. Discussion

This work has focused on using IR emissivity as a tool for measuring the response of materials to hydrogenation, an in-direct measurement of the presence of hydrogen in a material of interest. The experiments yielded an anticipated response, an increase of IR intensity when the material is expected to form hydride and decrease of IR intensity when hydrogen is expected to leave the material. The IR intensity was seen to be sensitive to local composition along the composition gradients and differences in a microstructure for

as-deposited and annealed films. As noted earlier, the relationships between IR emissivity and electrical resistivity and between resistivity and hydrogen presence in a metal predict the observed trend. Electrical resistivity is expected to increase with the formation of a hydrogen interstitial solid solution, increasing more significantly when the hydride phase starts to form; electrical resistivity of Mg films has been found to increase more then an order of magnitude during hydrogenation at 80 ˚C [20].

Other factors that can influence changes in IR emissivity during hydrogenation experiments should be also considered. This includes the effect of surface roughness on the emissivity [39, 40]. Significantly, this effect is negligible if the roughness is much smaller than the wavelength of emission. Formation of hydrides usually results in significant change in volume; Mg expands by 32% in volume when transforming from hcp Mg to rutile [41]. It is accepted that films usually accommodate the volume change by the expansion normal to a substrate. Such expansion could result in significant roughning of the film's surface. Indeed, for Mg films it was found with AFM an increase in the RMS roughness from 5 nm to 14 nm [41]. TEM examination of the films studied herein indicated that the roughness of the films after hydrogenation did not exceed 10 nm, well below the 1 to 5 μm light imaged by the IR camera. The impact of surface roughness on the measured IR signal is therefore believed to be negligible.

Another factor that could affect the intensity of IR emissivity is the temperature change resulting from heat evolution during the formation and decomposition of hydride phase(s). If the temperature change is detected, the measuring IR emissivity experiment becomes similar to DTA (Differential Thermal Analysis). In fact, one early work where IR imaging was used in hydrogenation experiments of Mg-Ni-Fe films, presented the results as an increase in temperature of the regions presumably reacting with hydrogen [9]. However, in the current experiments the rate of transformation is rather low, and both metallic films and a Si substrate being attached to a metallic heater provide good thermal conductivity with fast heat dissipation. The near constant level of IR intensity during the hydrogenation stage (after the initial rise), significantly above the pre-hydrogenation level, indicates that the intensity is an intrinsic property of the newly formed hydride, and not a result of increased temperature.

The formation of new phases, which are not hydrides, could also impact the IR emissivity. Examples could be interdiffusion reactions at elevated temperatures between capping Pd and a film, or between the substrate and film before formation of hydride started. Transformation of the as-deposited metastable phase to a more stable or equilibrium phase before the hydrogenation takes place is also possibility. However, any metallic phases would have electrical conductivity similar to that of the deposited film so no considerable effect on emissivity would be expected. More significantly, interdiffusion would be irreversible, as would such reactions in the temperatures being considered, and therefore inconsistent with the IR behavior observed during de-hydrogenation.

Based on the above considerations, interpretation of the measured changes in IR emissivity in terms of formation and growth of a hydride phase under hydrogen pressure,

and the reverse transformation to a metallic phase after removal of hydrogen pressure, appears correct. As such, interpretation of the IR intensity curves in Fig. 6 is as follow:

The initial fast increase in IR intensity shows the fast formation of a hydride layer below the thin layer of Pd (presumably transformed to PdH_2). Further moderate increase in the IR intensity corresponds to increases volume fraction of the hydride associated with thickening of this layer. However, saturation of the intensity, e.g. approximately after 1 h for the as-deposited film, would not necessarily indicate the completion of transformation in a film to 100 % hydride phase; it can also be an indication that the thickness of hydride is equal or larger than an escape depth of the IR radiation. However, our recent experiments with wedge-like films show that for Mg hydrite the escape depth is more then 500 nm. Secondary increase of the intensity at 0.5 MPa of hydrogen pressure for higher Ni compositions is interpreted as the formation of a new hydride from a secondary phase of the film, presumably Mg_2Ni transforming to Mg_2NiH_4. Similarity of the IR curves for different compositions suggests similar phases are involved in the transformations, namely the same metallic and hydride phases, over a broad range of compositions. Differences in the IR intensity level between high and low Mg compositions is believed to arise from different volume fractions of the hydride phase rather than any impact of composition on the intrinsic emissivity of the hydride.

After removal of hydrogen from a chamber, the measurements of the as-deposited film indicate that for higher Ni concentrations the decrease in IR intensity occurs at 150 °C and continues at 200 ˚C, whereas for higher Mg concentrations it only occurs at 200 °C. Also at 200 °C the intensity decrease is more prolonged (> 2 h) for higher Mg concentrations. The decrease at 150 °C for the former is attributed to dehydrogenation of intermetallic-based hydride, probably Mg_2NiH_4, and the decrease at 200 ˚C is attributed to decomposition of the main hydride phase.

The experiments show that moderate modification of structure by annealing at 250 ˚C can result in different absorption/desorption behavior as captured in the evolution of IR curves for the same set of experimental conditions. Mg-Ni films have been studied by a number of groups for their hydrogenation and optical properties [24-30]; however , this work appears to be the first to report the formation of a metastable Mg(Ni) fcc phase. Finding of the metastable fcc phase with nanosize grains came through electron diffraction and high-resolution TEM imaging studies. According to x-ray measurements, the microstructure of the films would be qualified as “x-ray amorphous”. Such “x-ray amorphous” Mg-Ni structures have been reported for different sputtered films (Mg=87 and 67 at%) [18, 24], and for the high-energy ball-milled powders [17, 29]. Thus it is possible that the nanostructure of the Mg fcc structure was not detected in other materials. Fcc structure is similar to hcp structure as both are close-packed structures of hexagonal layers in different stacking sequences. Thus free energies of the hcp and fcc structures are close, and the possibility of formation of a metastable (not ground state) structure in different non-equilibrium conditions exists. Indeed, fcc Mg has been observed in ultra-thin Mg films evaporated on different substrates [42-44] and has also been predicted theoretically [43, 45]. Calculated Mg fcc (or bct) structure has a lattice parameter a=0.45 nm, which can be also obtained from the interatomic distances in

(0001) close-packed plane of hcp Mg.

Alloying a Mg hcp phase with the element having an fcc structure increases likelihood of formation of a metastable Mg-based fcc phase and its competitiveness with stable intermetallic phase(s). In the case of the Mg-Ni gradient films deposited through multilayering technique, the nanolayers of fcc Ni may play a role of both promoting the nucleation of an fcc phase and stabilizing the phase after interdiffusion with Mg. Apparently similar stabilization of fcc structures has been observed through electron microscopy of multilayered films of Ti and Al [46,47]; although x-ray diffraction of the samples indicated that the Ti actually deposited in the equilibrium hcp phase, and the fcc phase was in fact TiH_2 that formed during TEM sample preparation [48]. If Vegard law holds, the lattice parameter of the fcc phase will be changing from 0.45 nm (pure Mg) to 0.352 nm (pure Ni); TEM measurements have determined a=0.43 nm for the composition of approximately 80 at% Mg, with further reduction in the lattice parameter with increase in Ni concentration. Considering the detected presence of Mg_2Ni and $MgNi_2$ intermetallic phases in higher Ni compositions, the lattice parameter of the fcc phase is not expected to exceed a certain value, which based on these measurements appears to be 0.41 nm.

With the metastable fcc phase as a major phase in the studied films, the question arises as to what is the structure of a hydride phase in the films after hydrogenation. For the previously studied Mg and Mg_2Ni films the structures of the hydrides are α-MgH_2 (of rutile type) and Mg_2NiH_4, respectively [19-30]. MgH_2 exists in a few other structural modifications, which can be formed at high pressures or non-equilibrium processing conditions [49-51]. One of the phases is β-MgH_2 CaF_2-type ($Pa\bar{3}$, a =0.466 nm), which is based on the fcc Mg host structure with hydrogen occupying octahedral interstitial sites. The structure was observed experimentally and its transition to α-MgH_2 was demonstrated theoretically [49]. In addition to β-MgH_2, hydrides based on a metal fcc structure but with 7:1 ordering of Ga_7Ge-type were synthesized using high pressure for Mg with different transition metals (TM), e.g., Ti, V, Nb [52-54]. These hydrides have stoicheometry close to $Mg_{6-7}TMH_{13-16}$, and hydrogen atoms occupy interstitial positions (tetrahedral sites for Mg_7TMH_{16} were identified by high-energy synchrotron structure analysis [52]). According to [54], the hydrogen atoms help to “glue together” metals that usually are immiscible in the fcc arrangement.

Considering the existence of described competing fcc-based Mg hydrides, one should consider the possibility that the metastable fcc Mg(Ni) phase transforms reversibly to an interstitial fluorite-type hydride, e.g. similar to PdH_2. If this is the case, faster kinetics and lower temperature of hydrogenation/desorption typically observed in films can be explained by an interstitial ordering type reaction rather then reconstructive reaction of MgH_2 or Mg_2NiH_4.

CONCLUSIONS

The IR emissivity imaging experiments with in-situ hydrogenation and desorption in vacuum of Mgx(Ni)1-x composition gradient films have convincingly demonstrated that

the method is able to capture reaction of the films with hydrogen gas by showing increase of IR intensity with absorption and decrease with desorption of hydrogen. The observed changes in IR emissivity correlate with the presence of hydrogen in the material as determined through changes in electrical resistivity according to the Hagen-Rubens relation. The method resolves different responses to hydrogenation for different compositions along the compositional gradient of the films, with resolution at least 2 at%. The method is also sensitive to minor microstructural differences, as was shown for as-deposited and 250 °C post-annealed films. According to the evolution of IR intensities, kinetics of hydrogenation for the MgxNi1-x were similar to those measured using optical and electrical resistivity methods by other research groups.

Based on the IR intensity increase, the highest hydrogenation at 0.1 MPa/150 °C occurs for higher Mg compositions (0.9>x>0.75), with desorption at 200°C. The level of intensity corresponds to a volume fraction of the hydride phase(s), although saturation of intensity is not necessarily a manifestation of completion of the transformation through the thickness of the film.

TEM study of the films shows that microstructure consists of the nanosize grains of a metastable fcc phase, with additional presence of Mg_2Ni and $MgNi_2$ phases at higher Ni compositions, throughout a broad range of compositions. The metastable phase appears to be a Ni-stabilized fcc form of Mg. Thus, hydrogenation differences between the studied film and bulk material, or films synthesized by different methods, should be interpreted not only in terms of microstructural differences (fine grains and disordered grain boundary region), but also with consideration of the initial phase and, perhaps, the hydride phase.

References:

1. X-D. Xiang, X. Sun, G. Brice, Y. Lou, K-A, Wang, H. Chang, W.G. Wallace-Freedman, S-W. Chen and P.G. Schultz, Science, 268 (1995) 1738

2. H. Koinuma and I. Takeuchi, Nature materials, 3 (2004) 429

3. J.-C. Zhao, Progress in Materials Science, 51 (2006) 557

4. Basic Research Needs for the Hydrogen Economy, US Department of Energy, p. 32 (http://www.sc.doe.gov/bes/hydrogen.pdf)

5. DoE 2007 Annual Progress Report, IV. Hydrogen Storage, http://www.hydrogen.energy.gov/annual_progress07_storage.html

6. R. Checchetto, G Trettel and A Miotello, Meas. Sci. Technol, 15 (2004) 127

7. B. Bogdanovic and M. Schwickardi, J. Alloys Comp., 1 (1997) 253

8. J. Chen, N. Kuriyama, Q. Xu, H.T. Takeshita, and T. Sakai, J. Phys. Chem. B, 105 (2001) 11214

9. C. Olk, G.G. Tibbetts, D. Simon and J.J. Moleski, J. Appl. Phys., 94, 720 (2003); C. Olk. Meas. Sci. Technol., 16 (2005) 14

10. J.-C. Zhao, 2007 Annual Merit Review Proceedings, http://www.hydrogen.energy.gov/pdfs/review07/st_16_zhao.pdf

11. A. Ludwig, J. Cao, A. Savan, M. Ehmann, J. Alloys Comp., 446 (2007) 517

12. B. Dam, R. Gremaud, C. Broedersz and R. Griessen, Scripta Materialia, 56 (2007) 853

13. R. Gremaud, C.P. Broedersz, D.M. Borsa, A. Borgschulte, P.Mauron, H. Schreuders, J.H. Rector, B. Dam, and R. Griessen, Adv. Mater., 19 (2007) 2813

14. J. N. Huiberts, R. Griessen, J. H. Rector, R. J. Wijngaarden, J. P. Dekker, D. G. De Groot, N. J. Koeman, Nature, 380 (1996) 231

15. T. F. Rosenbaum, A. F. T. Hoekstra, Adv. Mater., 14 (2002) 247

16. M. Dornheim, S. Doppiu, G. Barkhordarian, U. Boesenberg, T. Klassen, O. Gutfleisch and R. Bormann, Scripta Materialia, 56 (2007) 841

17. L. Zaluski, A. Zaluska, P. Tessier, J. O. Stromolsen, and R. Schulz, J. Alloys Comp., 217 (1995) 295

18. T. J. Richardson, J. L. Slack, B. Farangis, and M. D. Rubin, Appl. Phys. Lett., 80

(2002) 1349

19. K. Yamamoto, K. Higuchi, H. Kajioka, H. Sumida, S. Orimo, H. Fujii , J. Alloys Comp., 330–332 (2002) 352

20. A.S. Ingason, S. Olafsson, J. Alloys Comp., 404–406 (2005) 469

21. R. Kekekar, H. Giffard, S. T. Kelly, and B. M. Clemens, J. Appl. Phys., 101 (2007) 114311

22. I.A.M.E. Giebels, J. Isidorsson and R. Griessen, Phys. Rev. B, 69 (2004) 11

23. S. Singh, S.W.H. Eijt, M.W. Zandbergen, W.J. Legerstee, and V.L. Svetchnikov, J. Alloys Comp., 441 (2007) 344

24. B. Farangis, P. Nachimuthu, T.J. Richardson, J. L. Slack, R.C.C. Perera, E.M. Gullikson, D. W. Lindle, and M. Rubin, Phys. Rev. B, 67 (2003) 85106

25. W. Lohstroh, R. J. Westerwaal, J. L. van Mechelen, C. Chacon, E. Johansson, B. Dam, and R. Griessen, Phys. Rev. B, 70 (2004) 165411

26. K. Yoshimura, Y. Yamada, and M. Okada, Applied Physics Letters, 81 (2002) 4709

27. L.Z. Ouyang, S.Y. Ye, H.W. Dong, and M. Zhu, Applied Physics Letters, 90 (2007) 21917

28. J. Chen, H.-B. Yang, Y.-Y. Xia, N. Kuriyama, Q. Xu, and T. Sakai, Chem. Mater., 14 (2002) 2834

29. S. Orimo and H. Fujii, Appl. Phys. A, 72 (2001) 167

30. J. L. M. van Mechelen, B. Noheda, W. Lohstroh, R.J. Westerwaal, J.H. Rector, B. Dam, and R. Griessen, Appl. Phys. Lett., 84 (2004) 3651

31. L. D. Landau and E. M. Lifshitz, Statistical Physics, third ed., Pergamon, New York, 1980

32. N.F. Mott and H. Jones, The Theory of the Properties of Metals and Alloys, Oxford, 1936

33. A.V. Sokolov, Optical Properties of Metal*s,* American Elsevier Publ. Co., 1967

34. L. D. Landau and E. M. Lifshitz, Electrodynamics of Continuous Media, Pergamon, New York, 1960

35. B. Baranowsky, in: G. Alefeld, J. Volkl (Eds.), Hydrogen in Metals II, Springer-

Verlag, Berlin, Heiderlberg, 1978, pp. 157-198

36. M. Gupta and L. Schlapbach, in: L. Schlapbach (Ed.), Hydrogen in Intermetallic Compounds I, Springer-Verlag, Berlin, Heiderlberg, 1988

37. S. M. Stirk, S. M. Thompson, and J. A. D. Matthew, Appl. Phys. Lett., 86 (2005) 102505

38. K.-S. Chang, M. Aronova, O. O. Famodu, I. Takeuchi, S. E. Lofland, J.Hattrick-Simpers, and H. Chang, Appl. Phys. Lett., 79 (2001) 4411

39. L. Ibos, M. Marchetti, A. Boudenne, S. Datcu, Y. Candau and J. Livet, Measurement Science and Technology, 17 (2006) 2950

40. W. Sabuga and R. Todtenhaupt, High Temperatures-High Pressures, 33 (2001) 261

41. J. Isidorsson, I. A. M. E. Giebels, H. Arwin, and R. Griessen, Phys. Rev. B, 68 (2003) 13

42. M.C. Gallagher, Phys. Rev. B, 59 (1999) 2346

43. X Z Ji and F Jona, J. Phys.: Condens. Matter., 14 (2002) 12451

44. A. P. Janssen, R. C. Schoonmaker, and A. Chambers, Surf. Sci. 49 (1975) 143

45. F. Jona and P.M. Marcus, Phys. Rev. B, 66 (2002) 94104; F. Jona and P.M. Marcus, J. Phys.-Condensed Matt., 15 (2003) 7727

46. D. van Heerden, D. Josell, and D. Shechtman, Acta Mater., 44 (1996) 297

47. R. Banerjee, S.A. Dregia, and H.L. Fraser *Acta Mater.,* 47 (1999) 4225

48. J. Bonevich and D. Josell *Phys. Rev. Lett.,* 82 (1999) 2002

49. P. Vajeeston, P. Ravindran, A. Kjekshus, H. Fjellvåg, Phys. Rev. Lett., 89 (2002) 175506; P. Vajeeston, P. Ravindran, B. C. Hauback, H. Fjellvåg, A. Kjekshus, S. Furuseth, and M. Hanfland , Phys. Rev. B, 73 (2006) 224102

50. Y. Song and Z. X. Guo, Appl. Phys. Lett., 89 (2006) 111911

51. F. Cleri, M. Celino, A. Montone, E. Bonetti and L. Pasquini, Materials Science Forum, 555 (2007) 349

52. E. Ronnebro, D. Kyoi, A. Kitano, Y. Kitano, and T. Sakai, J. Alloys and Comp., 404-406 (2005) 68

53. D. Kyoi, N. Kitamura, H. Tanaka, A. Ueda, S. Tanase, and T. Sakai, J. Alloys and Comp., 428 (2007) 268; D Kyoi, T Sato, E Ronnebro, Y. Tsuji, N. Kitamura, A. Ueda, M. Ito, S. Katsuyama, S. Hara, D. Noreus, and T. Sakai, J. Alloys and Comp., 375 (2004) 253; T. Takasaki, D. Kyoi, N. Kitamura, S. Tanase, and T. Sakai, Materials Science Forum, 561 (2007) 1577

54. T Sato, D Kyoi, E Ronnebro, N. Kitamura, T. Sakai, and D, Noreus, J. Alloys and Comp., 417 (2006) 230

Figures.

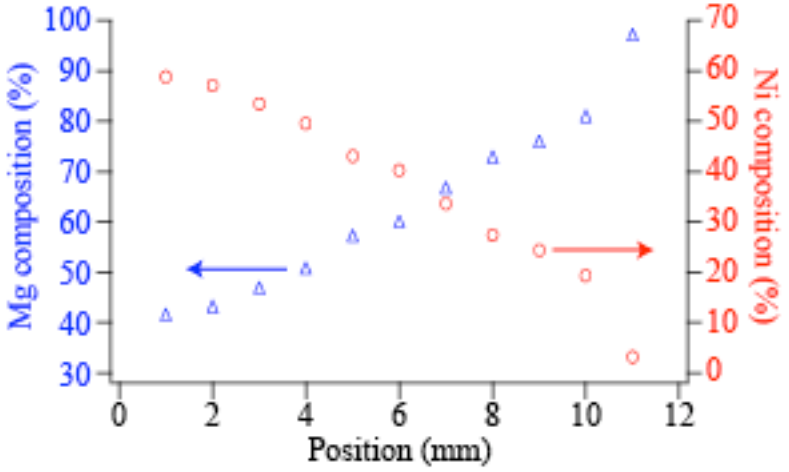

Fig. 1. Compositional variation across the film as measured by EDS.

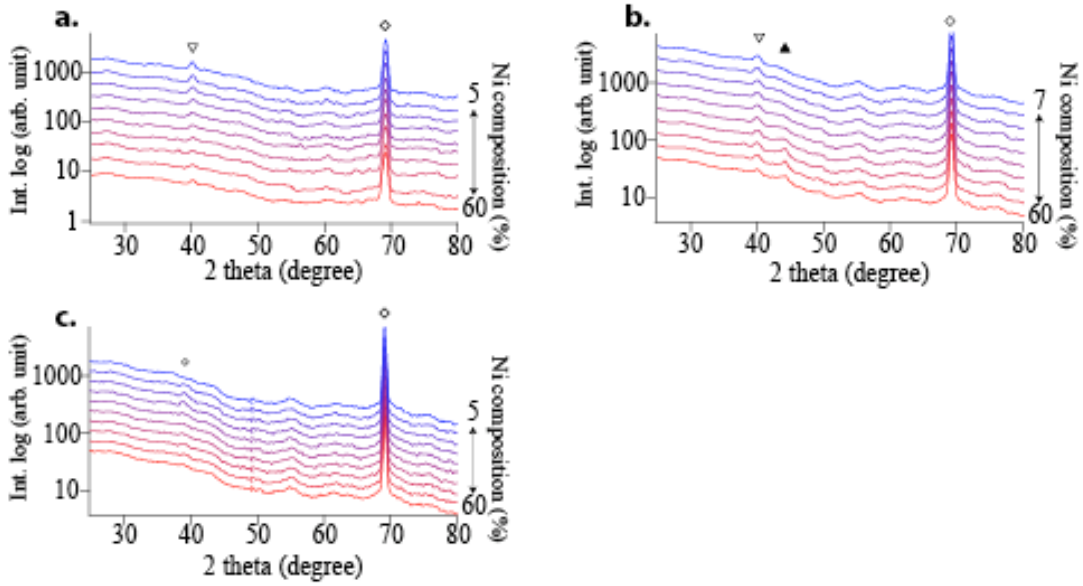

Fig. 2. XRD scans of Mg-Ni films: (a) as-deposited; (b) deposited and annealed at 250 ˚C; (c) as-deposited, after hydrogenation/dehydrogenation cycle at 150-200 ˚C.

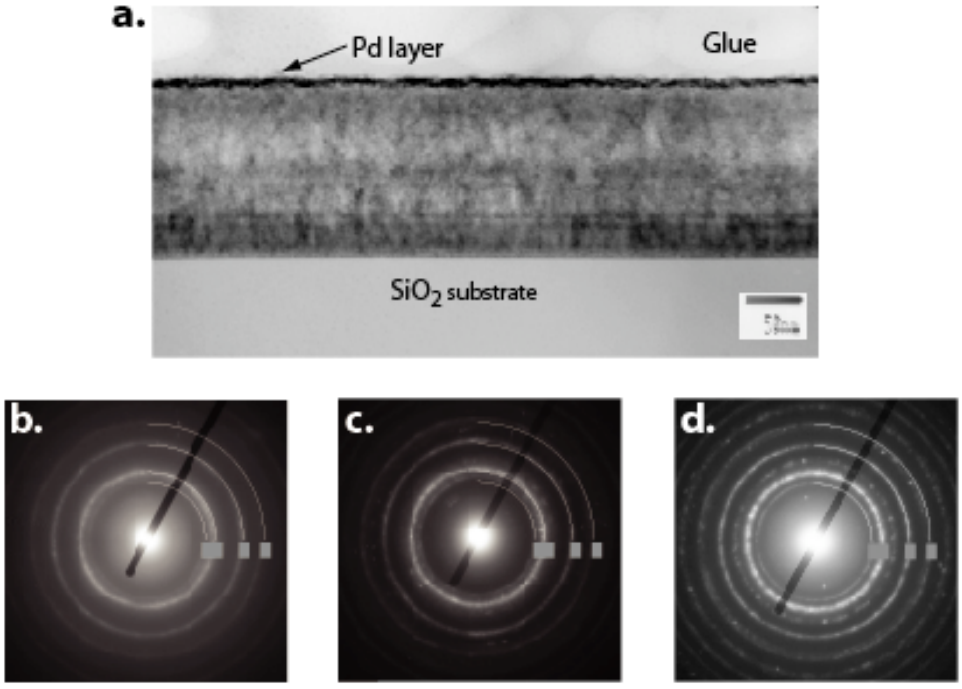

Fig. 3. TEM of the Mg-Ni 250 ˚C annealed film. (a) Bright field image of a cross section corresponding to 21 at % Ni composition (#4 section). (b-d) SAED patterns taken from the cross sections of 21, 43 and 60 at % Ni compositions, respectively.

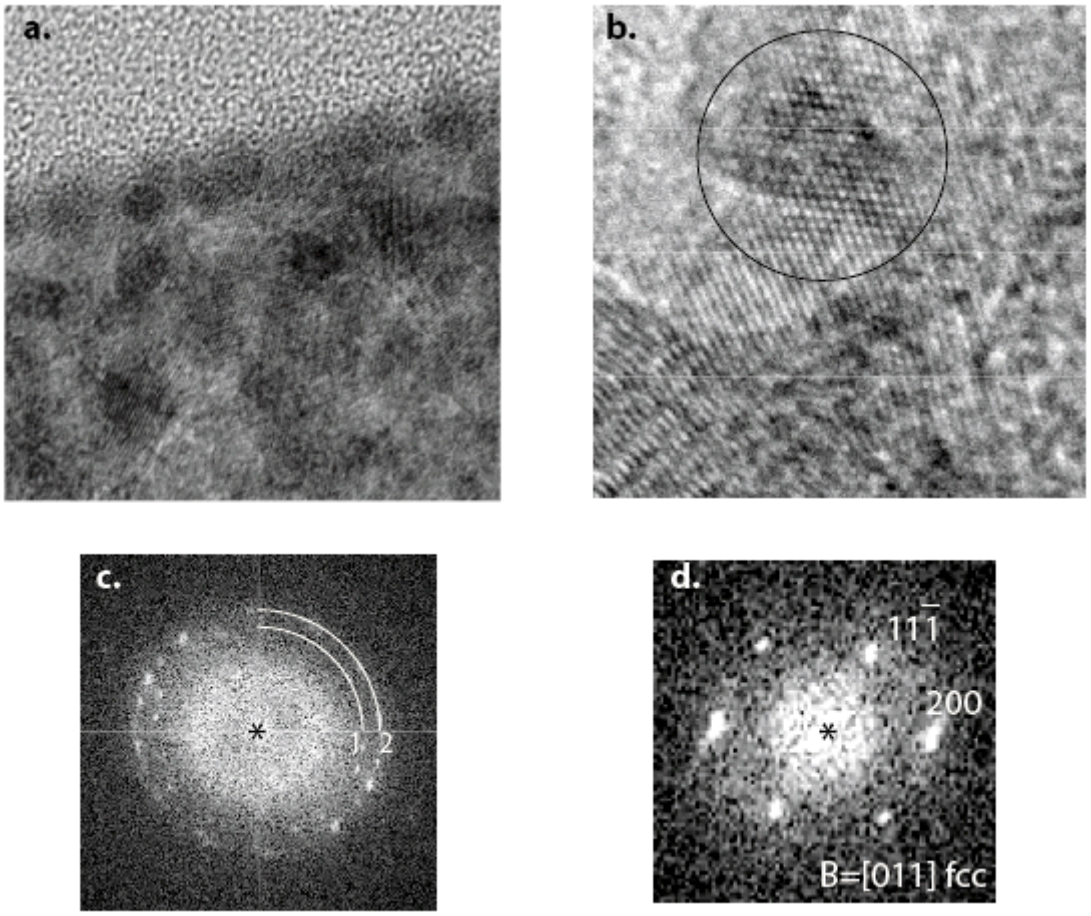

Fig. 4. High-resolution TEM images (a, b) and corresponding Fast Fourier Transforms (c, d) obtained from the Mg-Ni 250 ˚C annealed film of 21 at% Ni cross-section. Image in (b) shows a phase contrast typical for the [011]-oriented fcc structure

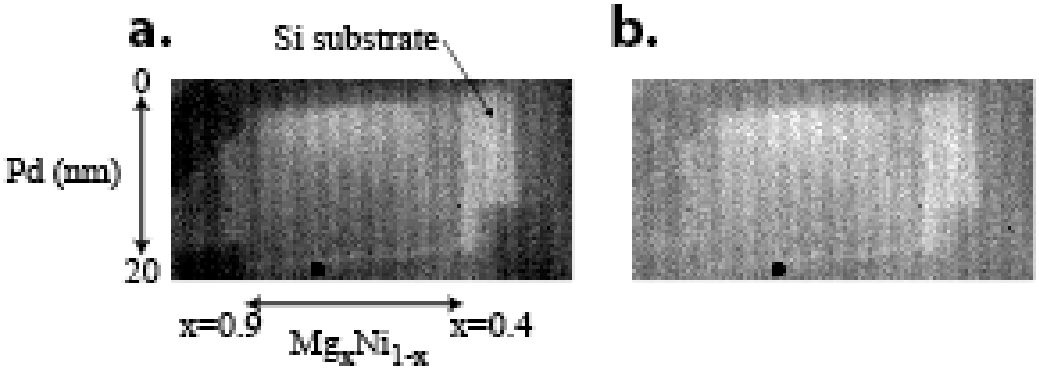

Fig. 5. Two IR images acquired before and after hydrogenation: (a) image was taken after the sample was equilibrated at 150 ˚C for one hour in vacuum, and (b) image was taken after the sample was exposed at 150 ˚C to hydrogen pressure of up to 5 atm for 3 hs.

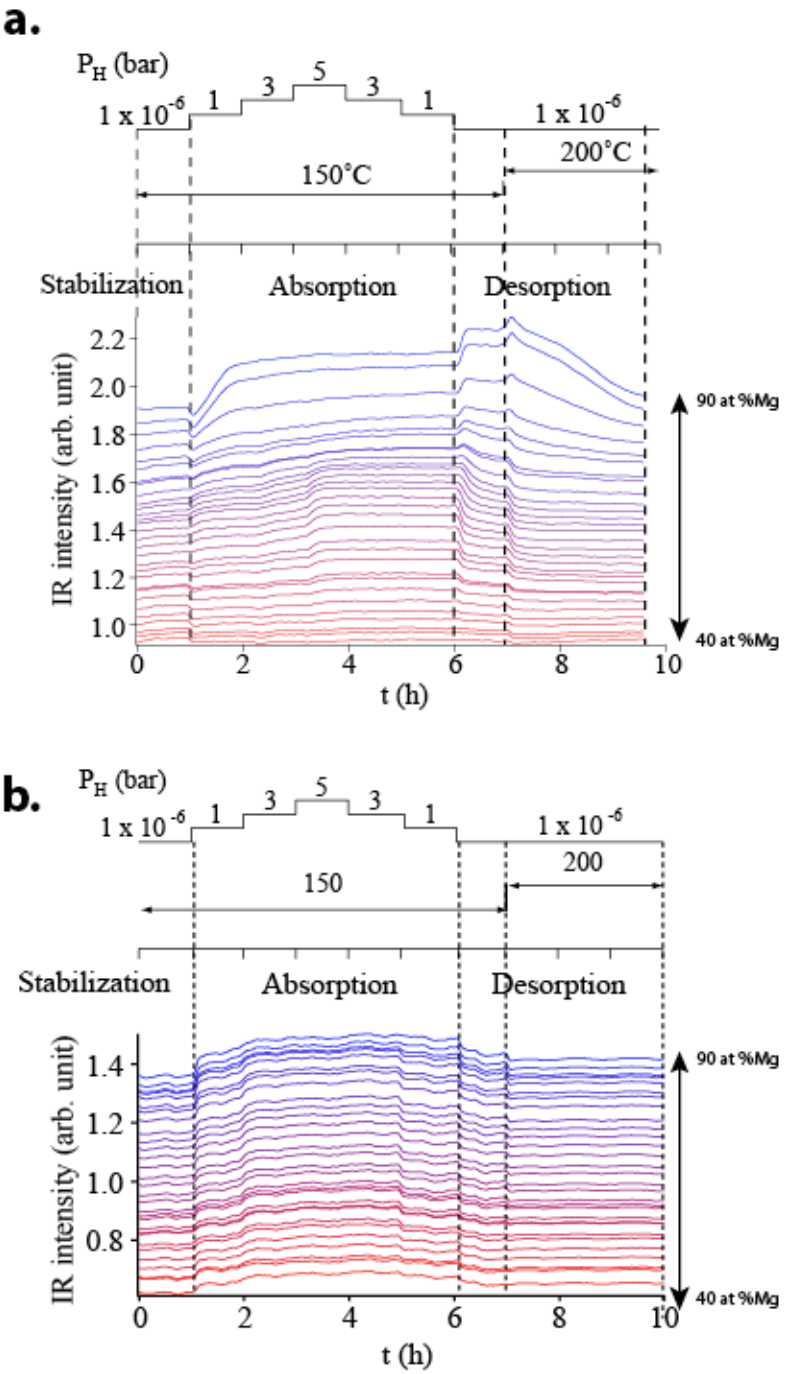

Fig. 6. Normalized IR intensity of as-deposited Mg_xNi_{1-x} (a) and annealed Mg_xNi_{1-x} (b). Equally spaced 30 measurement points along composition spread are chosen from one edge to another edge for each sample. By applying vertical offset, 30 normalized IR intensity curves as a function of measurement time are aligned to present results for all compositions, with higher Mg concentrations on top of each figure. On the right side of each figure the composition range is shown. On top of each figure the experimental schedule showing changes in H_2 pressure and temperature of samples is aligned with IR measurements.